

Probing hairy black holes caused by gravitational decoupling using quasinormal modes and greybody bounds

Yi Yang^{1,*}, Dong Liu^{1,†}, Ali Övgün^{2,‡}, Zheng-Wen Long^{1,§} and Zhaoyi Xu^{1,||}

¹*College of Physics, Guizhou University, Guiyang 550025, China*

²*Physics Department, Eastern Mediterranean University, Famagusta, 99628 North Cyprus via Mersin 10, Turkey*

 (Received 16 February 2023; accepted 19 February 2023; published 21 March 2023)

Gravitational decoupling can add hair to the black holes by adding extra sources. The quasinormal modes of a hairy black hole caused by gravitational decoupling for the massless scalar field, electromagnetic field, and gravitational perturbation are investigated. The equations of the effective potential for three perturbations are derived in a hairy black hole spacetime. We also study the time evolution corresponding to the three perturbations, and the quasinormal mode frequencies are calculated using the Prony method through the time-domain profiles. By analyzing the influence of the hairs (α , l_0 and Q) for the black holes we are studying on quasinormal modes, we find that the hairs α and l_0 decrease the oscillation frequency of the gravitational-wave signal, and the hair Q increases its oscillation frequency. Furthermore, we calculate the bounds of the greybody factor and high-energy absorption cross section with the sinc approximation, which reveals that the presence of charges (α and l_0) generating primary hair can increase the probability of gravitational radiation arriving at spatial infinity, whereas the charge Q from the extra sources does the opposite.

DOI: [10.1103/PhysRevD.107.064042](https://doi.org/10.1103/PhysRevD.107.064042)

I. INTRODUCTION

General relativity shows that when a massive star collapses into a black hole, there are only three physical quantities—mass, angular momentum, and electric charge—which uniquely determine the properties of the black hole. All the other information (“hair”) disappears [1,2]. However, there may be some other physical quantities that describe black holes. For example, a black hole may also have quantum hairs [3]. Many methods are used to evade the no-hair theorem [4–8]. In particular, Ovalle proposed a gravitational decoupling method to obtain the solutions of the Einstein field equations by decoupling of the gravitational sources [9,10]. The gravitational decoupling method has gained a lot of attention [11–23] mainly, because it has the following advantages: (i) it can decouple the complex energy-momentum tensor into relatively simpler components; (ii) one can use it to extend some known seed solutions to more complex solutions; and (iii) one can use it to find solutions of gravitational theories other than general relativity. Ovalle *et al.* assumed that there are additional general sources described by the conserved

energy-momentum tensor $\theta_{\mu\nu}$. This $\theta_{\mu\nu}$ can explain one or more fundamental fields, and its key property is that it is subject to gravity but does not directly interact with the matter of the black hole. Then, they obtained the hairy black hole solution by gravitational decoupling [24,25]. In particular, two new families of hairy black holes were discovered by Ovalle *et al.* in Ref. [25], which demonstrates that basic deformations of the seeded Schwarzschild vacuum retain the energy conditions, and proposes a novel method for evading the no-hair theorem depending on a primary hair correlated with the charge that generates these transformations. This leads us to be interested in the stability of such a hairy black hole.

The stability of a black hole under certain perturbations is closely related to the properties of the black hole itself. Usually, the stability of a black hole spacetime under perturbations is studied through the field evolution of the black hole background or a black hole merger. A perturbed black hole can emit gravitational waves (GW), which are dominated by quasinormal modes (QNMs) [26] with a complex frequency, where the real part of the QNM frequency denotes the oscillation frequency of the black hole when perturbed, and the imaginary part represents the decay rate [27–32]. In addition to characterizing the stability of a black hole spacetime, the QNM frequency also plays a very important role in determining black hole parameters. Moreover, a collision event between black holes will go through three phases: inspiral, merger and ringdown phases. LIGO/VIRGO first observed gravitational

* yangyigz@yeah.net

† dongliuvv@yeah.net

‡ ali.ovgun@emu.edu.tr

§ Corresponding author.

zwlong@gzu.edu.cn

|| zyxu@gzu.edu.cn

waves produced from the black hole merger in 2016 [33]. They found a ringdown in the gravitational-wave signal, which appears at the end of the waveform and consists of rapidly decaying oscillations. The ringdown phase is the QNM of the remnant black hole, which has generated great interest in the study of black hole QNMs. In Ref. [34], Cheung *et al.* studied the QNM spectrum in which the Schwarzschild potential is perturbed by a small “bump” consisting of the Gaussian potential or the Pöschl-Teller potential, and they demonstrated that the fundamental mode is unstable under general perturbations. In Ref. [35], the authors studied the pseudospectrum of horizonless exotic compact objects (ECOs) with reflective surfaces close to the Schwarzschild radius, and demonstrated that the QNMs of ECOs are affected by the overall spectral instability. In Ref. [36], the authors studied the stability of a black hole with scalar hair under axial gravitational perturbations, and they found that this black hole with scalar hair is linearly stable. In particular, Cardoso *et al.* pointed out that the QNM spectra of some compact objects with light rings are radically different from that of a black hole, but they still show a similar ringdown stage [37]. In fact, this especial QNM spectrum is also known as echoes [38–51]. Numerous studies have shown that the QNM frequency of a black hole is only determined by the properties of the black hole itself and fields [52–72]. Therefore, we believe that the properties of a hairy black hole with additional sources described by a conserved energy-momentum tensor can be inspected through the QNM.

Quantum mechanics and general relativity form the bedrock of the current understanding of physics, but the two theories do not work together. In 1974, Hawking showed that black holes are not perfectly “black” but actually emit particles [73,74] as well as scatter and absorb radiation. Hawking radiation propagates on the curved spacetime due to the black hole, and the curvature of spacetime behaves like a gravitational potential where the radiation is scattered from it. There are two parts: (i) reflected back into black hole and (ii) transmitted to spatial infinity. Hence one can calculate the transmission probability, known as the greybody factor, using various methods such as the matching technique [75], the WKB approximation for a high gravitational potential [76,77] and using the rigorous bound [78–80]. On the other hand, the evaporation rate is proportional to the total absorption cross section. Since Hawking’s discovery, there have been many studies done on the absorption cross section of scalar fields in a black hole spacetime. First Sanchez [81] calculated the absorption cross section of a massless scalar wave for the Schwarzschild black hole in the high-frequency regime, which exhibits oscillation around the geometrical optics limit using numerical methods. It is known that the low-frequency behavior of the scalar field absorption by a black hole tends to the surface area of the event horizon [82]. At high energy, the absorption cross section oscillates around a limiting constant

value. For a scalar field absorbed by a spherically symmetric black hole, using complex angular momentum methods, Decanini *et al.* derived Sanchez’s result in the high-frequency regime with a more accurate coefficient. They obtained the absorption cross section using the sinc function $\sigma_{abs} = -8\pi e^{-\pi} \sigma_{geo} \text{sinc}[2\pi(3\sqrt{3}M)\omega]$, with $\text{sinc}(x) = (\sin x)/x$ and $\sigma_{geo} = 27\pi M^2$ which are related to the properties of the unstable photon orbit [83,84]. In the high-frequency approximation, it was shown that the oscillatory term arises from a sum of Regge poles which are characteristic resonances of the spacetime related to the QNMs. Briefly, the sinc approximation describes numerically and physically the fluctuations of the high-energy absorption cross section.

The authors of Ref. [85] studied the behavior of the hairy black hole in Ref. [25] under scalar field perturbation, which proved QNM frequencies regulated by the hair. The main goal of this paper is to probe the physical properties of another hairy black hole from Ref. [25] caused by gravitational decoupling using quasinormal modes under a massless scalar field, electromagnetic field and axial gravitational perturbations. This involves thorough calculations of how to see the effect of hair on QNM frequencies and time-domain profiles. The second goal is to study the greybody bound of hairy black hole caused by gravitational decoupling. To that end, we show numerically how the hair appears in the greybody bounds, as well as the high-energy absorption cross section with the sinc approximation.

This paper is organized as follows. In the next section we briefly review a hairy black hole caused by gravitational decoupling. Furthermore, we analyze the scalar field, electromagnetic field, and axial gravitational perturbations in the hairy black hole background spacetime. In Sec. III, the time-domain profiles of a massless scalar field, electromagnetic field and axial gravitational perturbations in a hairy black hole spacetime are given, and we also calculate the QNM frequencies using the Prony method and the 6th- and 13th-order WKB methods. In Sec. IV, the greybody factors and high-energy absorption cross section via the sinc approximation are discussed. Section V is a conclusion of the full text and a brief discussion of future directions.

II. EXTERNAL FIELDS AND AXIAL GRAVITATIONAL PERTURBATIONS IN HAIRY BLACK HOLE SPACETIME

A. Brief review of the hairy black hole

Ovalle *et al.* used gravitational decoupling to give a spherically symmetric black hole with scalar hairs. This method has two characteristics: extending simple solutions to more complex fields and decoupling some complex sources of gravity. They assumed that the system has a well-defined event horizon and the conserved

energy-momentum tensor describing the additional source satisfies the strong energy condition or dominant energy condition outside the event horizon [25]. The metric has the form ($G = c = 1$)

$$ds^2 = e^{\nu(r)} dt^2 - e^{\lambda(r)} dr^2 - r^2(d\theta^2 + \sin^2\theta d\phi^2), \quad (1)$$

where

$$e^\nu = e^{-\lambda} = 1 - \frac{2\mathcal{M}}{r} + \alpha e^{-r/(\mathcal{M}-\alpha l_0/2)}, \quad (2)$$

where \mathcal{M} is an asymptotic mass $\mathcal{M} = M + \alpha l_0/2$. This solution is presented by using gravitational decoupling and the strong energy condition. Moreover, using the dominant energy condition, the ‘‘charged’’ hairy black hole can be written as [25]

$$e^\nu = e^{-\lambda} = 1 - \frac{2M + \alpha l_0}{r} + \frac{Q^2}{r^2} - \frac{\alpha M e^{-r/M}}{r}. \quad (3)$$

The solution (2) has been studied in detail by Cavalcanti *et al.* [85]. Therefore, all the content we give in the following is for the black hole (3), and we will not discuss the relevant content of the black hole (2). It is worth noting that we cannot reduce the hairy black hole (3) to Eq. (2) by setting $Q = 0$. The main reason is that the black hole solution (2) is the Schwarzschild deformation produced by a gravitational source which satisfies the strong energy conditions, while the black hole solution (3) is produced by a generic source satisfying the dominant energy conditions [25]. For the ‘‘charged’’ hairy black hole (3), the event horizon radius r_h is given by the solution of the following equation:

$$r_h = \alpha l_0 + 2M - \frac{Q^2}{r_h} + \alpha M e^{-r_h/M}. \quad (4)$$

In addition, Ref. [25] pointed out that the hairs Q , α , and l_0 of the hairy black hole (3) satisfy the following relationship:

$$Q^2 \geq 4\alpha(M/e)^2 \quad \text{and} \quad l_0 \geq M/e^2. \quad (5)$$

From Eq. (5) we can see that the case where $Q = 0$ and α is nonzero is not allowed. Therefore, we do not discuss this case in this work. It should be noted that some regions of the parameter space will make hairy black holes (3) become a naked singularity. For example, when $Q > M$ with $a = 0$, hairy black holes (3) become a naked singularity. Therefore, there should be a minimum α that turns the naked singularity into a black hole with an event horizon.

This hairy black hole (3) contains parameters Q , M , l_0 , α , where $\{Q, \Delta = \alpha l_0\}$ denotes a potential set of charges generating primary hair. It should be noted that the charge Q is not necessarily an electric charge of the Maxwell field source, because the source for the charge Q is a tensor vacuum. The charge Q could be a tidal charge of extra-dimensional origin or any other source. However, when the charge Q denotes an electric charge, one can say that the electrovacuum of the Reissner-Nordström geometry also includes a tensor vacuum [25]. There are many similar examples. For example, the hair Q is not an electric charge in the Dadhich-Maartens-Papadopoulos-Rezania black hole solution [86], whose charge Q is associated with a conformal theory. In particular, the parameter Δ is closely related to the gauge transformation of the Schwarzschild metric, and it can push the event horizon to a place larger than the Schwarzschild radius, such that it can measure how much the black hole’s entropy increases relative to the minimum Schwarzschild value as the black hole hair is added [25].

B. Scalar perturbation of the hairy black hole

In the context of general relativity, there are two methods to study the black hole perturbations. The first method is to include a test field in the black hole background and to study the system by solving the dynamical equation for a specific test field in the black hole background. The second is the perturbation metric itself, i.e. the gravitational perturbation, in which the evolution equation is usually found by linearizing the Einstein equations. The most important feature between the two methods is that the gravitational radiation excited by gravitational perturbation is much stronger than the gravitational radiation excited by the perturbation of the external field of the black hole. We will first study the case where the external field is a scalar field. In curved spacetime, the perturbation equation of the massless scalar field can be written as

$$\frac{1}{\sqrt{-g}} \partial_\mu (\sqrt{-g} g^{\mu\nu} \partial_\nu \Psi) = 0. \quad (6)$$

Putting our considered hairy black hole metric into the scalar field equation, we can get

$$-\frac{\partial_t^2 \Psi}{e^\nu} + \frac{1}{r^2} (2re^\nu \partial_r \Psi + r^2 e^\nu \partial_r \Psi + r^2 e^\nu \partial_r^2 \Psi) + \frac{1}{r^2} \left(\frac{1}{\sin\theta} \partial_\theta \sin\theta \partial_\theta \Psi + \frac{1}{\sin^2\theta} \partial_\phi^2 \Psi \right) = 0, \quad (7)$$

where $e^{\nu'}$ denote $\frac{d}{dr} e^\nu$. Due to the symmetry of the hairy black hole spacetime background, we perform separation of variables

$$\Psi(t, r, \theta, \phi) = \sum_{l,m} \psi(t, r) Y_{lm}(\theta, \phi) / r, \quad (8)$$

by substituting it into Eq. (7), we can get the second-order partial differential equation about the tortoise coordinate in the scalar field perturbation

$$\frac{d\psi^2}{dt^2} - \frac{d\psi^2}{d\tau^2} + V(r)\psi = 0, \quad (9)$$

where the tortoise coordinate τ is defined as $d\tau = 1/e^\nu dr$, and $V(r)$ is the effective potential

$$V(r) = \left(1 - \frac{2M + \alpha l_0}{r} + \frac{Q^2}{r^2} + \frac{\alpha M e^{-r/M}}{r} \right) \times \left[\frac{l(l+1)}{r^2} - \frac{2Q^2}{r^4} + \frac{2M}{r^3} + \frac{M\alpha e^{-r/M}}{r^3} + \frac{\alpha e^{-r/M}}{r^2} + \frac{\alpha l_0}{r^3} \right]. \quad (10)$$

The perturbation of the scalar field has been receiving more attention. Moderski *et al.* have investigated the QNM spectrum under the perturbation of the scalar field in different black hole spacetimes [87–89]. Boudet *et al.* have examined the QNM for a Schwarzschild black hole under projective-invariant Chern-Simons modified gravity [90]. The authors of Ref. [91] investigated the QNM of a scalar field perturbation in the spacetime of a rotating regular black hole.

C. Electromagnetic perturbation of the hairy black hole

The Maxwell equation satisfied by the electromagnetic field is

$$\frac{1}{\sqrt{-g}} \partial_{x^\nu} (\sqrt{-g} F^{\mu\nu}) = J^\mu. \quad (11)$$

The electromagnetic field we are studying is a vacuum, so the value of the four-current density J^μ is 0. $F^{\mu\nu}$ is the contravariant tensor of the electromagnetic field in the black hole spacetime background, and its covariant tensor is

$$F_{\mu\nu} = A_{\nu,\mu} - A_{\mu,\nu}, \quad (12)$$

where the comma denotes the ordinary derivative. Since the background we are studying is spherically symmetric, A_μ can be expanded in the four-dimensional vector spherical harmonics as [92]

$$A_\mu(t, r, \theta, \phi) = \sum_{l,m} \left(\begin{array}{c} 0 \\ 0 \\ b^{lm}(t, r) \frac{1}{\sin\theta} \partial_\phi Y_{lm} \\ -b^{lm}(t, r) \sin\theta \partial_\theta Y_{lm} \\ f^{lm}(t, r) Y_{lm} \\ h^{lm}(t, r) Y_{lm} \\ k^{lm}(t, r) \partial_\theta Y_{lm} \\ k^{lm}(t, r) \partial_\phi Y_{lm} \end{array} \right), \quad (13)$$

with l being the angular quantum number, and m being the azimuthal number. The item on the left has parity $(-1)^{l+1}$, and the item on the right has parity $(-1)^l$. Moreover, Y_{lm} are the spherical harmonics. Substituting Eq. (13) into Maxwell's equation (11), and using the tortoise coordinate, the second-order differential equation for the perturbation can be obtained as

$$\frac{d\psi^2}{dt^2} - \frac{d\psi^2}{d\tau^2} + V(r)\psi = 0, \quad (14)$$

where the wave function $\psi(r)$ is a linear combination of b^{lm} , f^{lm} , h^{lm} and k^{lm} , and the effective potential of the electromagnetic field perturbation in the hairy black hole spacetime is

$$V(r) = \left(1 - \frac{2M + \alpha l_0}{r} + \frac{Q^2}{r^2} + \frac{\alpha M e^{-r/M}}{r} \right) \left[\frac{l(l+1)}{r^2} \right]. \quad (15)$$

D. Axial gravitational perturbations of the hairy black hole

Regge and Wheeler were the first to study the axial gravitational perturbation of a Schwarzschild black hole [93]. The standard procedure for axial gravitational perturbation is to introduce a small perturbation $h_{\mu\nu}$ into the static background metric $g_{\mu\nu}^0$, i.e.

$$g_{\mu\nu} = g_{\mu\nu}^0 + h_{\mu\nu}, |h_{\mu\nu}| \ll 1. \quad (16)$$

Moreover, the Ricci tensor can be expressed as

$$R_{\mu\nu} = R_{\mu\nu}^0 + \delta R_{\mu\nu}, \quad (17)$$

with

$$\delta R_{\mu\nu} = \delta \Gamma_{\mu\alpha\nu}^\alpha - \delta \Gamma_{\mu\nu\alpha}^\alpha, \quad (18)$$

where

$$\delta \Gamma_{\mu\nu}^\beta = \frac{1}{2} g^{\beta\alpha} (h_{\alpha\nu;\mu} + h_{\alpha\mu;\nu} - h_{\mu\nu;\alpha}). \quad (19)$$

Regge and Wheeler proved that if the metric perturbation tensor $h_{\mu\nu}$ is expanded into tensor spherical harmonics, the equations describing the axial perturbations can be separated. Using the gauge symmetry of the field equations, one can obtain the general form of $h_{\mu\nu}$. The remaining components after simplification are [93]

$$h_{\mu\nu} = \begin{pmatrix} 0 & 0 & 0 & h_0(t, r) \\ 0 & 0 & 0 & h_1(t, r) \\ 0 & 0 & 0 & 0 \\ h_0(t, r) & h_1(t, r) & 0 & 0 \end{pmatrix} \sin\theta \partial_\theta P_\ell(\cos\theta), \quad (20)$$

with $P_\ell(\cos\theta)$ being the Legendre polynomial of order ℓ . Unknown functions $h_0(t, r)$ and $h_1(t, r)$ satisfy the following equations:

$$\frac{1}{f(r)} \frac{dh_0}{dt} - \frac{df(r)}{dr} h_1 - \frac{dh_1}{dr} f(r) = 0, \quad (21)$$

$$\left(\frac{d^2 h_1}{dt^2} - \frac{d^2 h_0}{dt dr} + \frac{2}{r} \frac{dh_0}{dt} \right) \frac{1}{f(r)} + \frac{l^2 + l - 2}{r^2} h_1 = 0, \quad (22)$$

$$\begin{aligned} & \left(\frac{d^2 h_0}{dr^2} - \frac{d^2 h_1}{dt dr} - \frac{2}{r} \frac{dh_1}{dt} \right) \frac{f(r)}{2} \\ & + \frac{h_0}{r^2} \left[r \frac{df(r)}{dr} - \frac{1}{2} l(l+1) \right] = 0, \end{aligned} \quad (23)$$

where $f(r)$ is the g_{tt} in the spherical symmetry metric. By defining $\Psi(t, r) = (1/r)f(r)h_1(t, r)$, and according to the tortoise coordinate, we can gain the Schrödinger-like equation of the axial gravitational perturbation

$$\frac{d\Psi^2}{dt^2} - \frac{d\Psi^2}{d\tau^2} + V(r)\Psi = 0, \quad (24)$$

where the Regge-Wheeler potential $V(r)$ can be read as

$$V(r) = \left(1 - \frac{2M + \alpha l_0}{r} + \frac{Q^2}{r^2} + \frac{\alpha M e^{-r/M}}{r} \right) \left[\frac{l(l+1)}{r^2} + \frac{4Q^2}{r^4} - \frac{6M}{r^3} - \frac{3M\alpha e^{-r/M}}{r^3} - \frac{\alpha e^{-r/M}}{r^2} - \frac{3\alpha l_0}{r^3} \right]. \quad (25)$$

III. QNM OF A HAIRY BLACK HOLE

In this section, we will numerically solve the wave equation in a hairy black hole spacetime background to gain the time-domain profiles of this spacetime. In addition, we use the Prony method to extract quasinormal modes, and our results are in good agreement with those calculated using the higher-order WKB method. To obtain the time-domain profiles of the hairy black hole, we introduce the light-cone coordinates

$$\begin{aligned} u &= t - \tau, \\ v &= t + \tau. \end{aligned} \quad (26)$$

Then Eq. (9) can be written as

$$\frac{\partial^2}{\partial u \partial v} \psi(u, v) = -\frac{1}{4} V(r) \psi(u, v). \quad (27)$$

Equation (27) can be discretized as [94,95]

$$\psi_N = \psi_E + \psi_W - \psi_S - \delta u \delta v V \left(\frac{\psi_W + \psi_E}{8} \right) + O(\Delta^4). \quad (28)$$

where $S = (u, v)$, $W = (u + \delta u, v)$, $E = (u, v + \delta v)$, $N = (u + \delta u, v + \delta v)$. Moreover, we use the following initial Gaussian pulse:

$$\begin{aligned} \psi(u = u_0, v) &= \exp \left[-\frac{(v - v_c)^2}{2\sigma^2} \right], \\ \psi(u, v = v_0) &= 0, \end{aligned} \quad (29)$$

where $u_0 = v_0 = 0, \sigma = 3, v_c = 10$. Thus, the time-domain profiles of a hairy black hole caused by gravitational decoupling can be obtained.

In Figs. 1 and 2, we show the time-domain profiles (TDPs) of the scalar field perturbation in the hairy black hole. The difference between these two figures is that we study the case of $l = 0$ in the former, and the case of $l = 1$ in the latter. In the top panels of Fig. 1 and Fig. 2, we show the influence of the black hole parameter α on the TDP, where $M = 1, l_0 = 1, Q = 0.7$. In addition, we also give the TDP of the Schwarzschild black hole. One can find that when α is the smallest, its damped is the strongest. In other words, the decay rate is the fastest when α is the smallest, which implies that the imaginary part of the QNM frequency will decrease as α increases. In the middle panels of Fig. 1 and Fig. 2, we give the influence of the hairy black hole charge l_0 on its TDP with $M = 1, \alpha = 0.9, Q = 0.7$. It shows that as l_0 increases, the TDP damping becomes slower, which is an indication that the imaginary part of the QNM frequency that denotes damping should also be decreasing when the charge l_0 increases. In the bottom panels of Fig. 1 and Fig. 2, the influence of the charge Q on the hairy black hole is presented, where

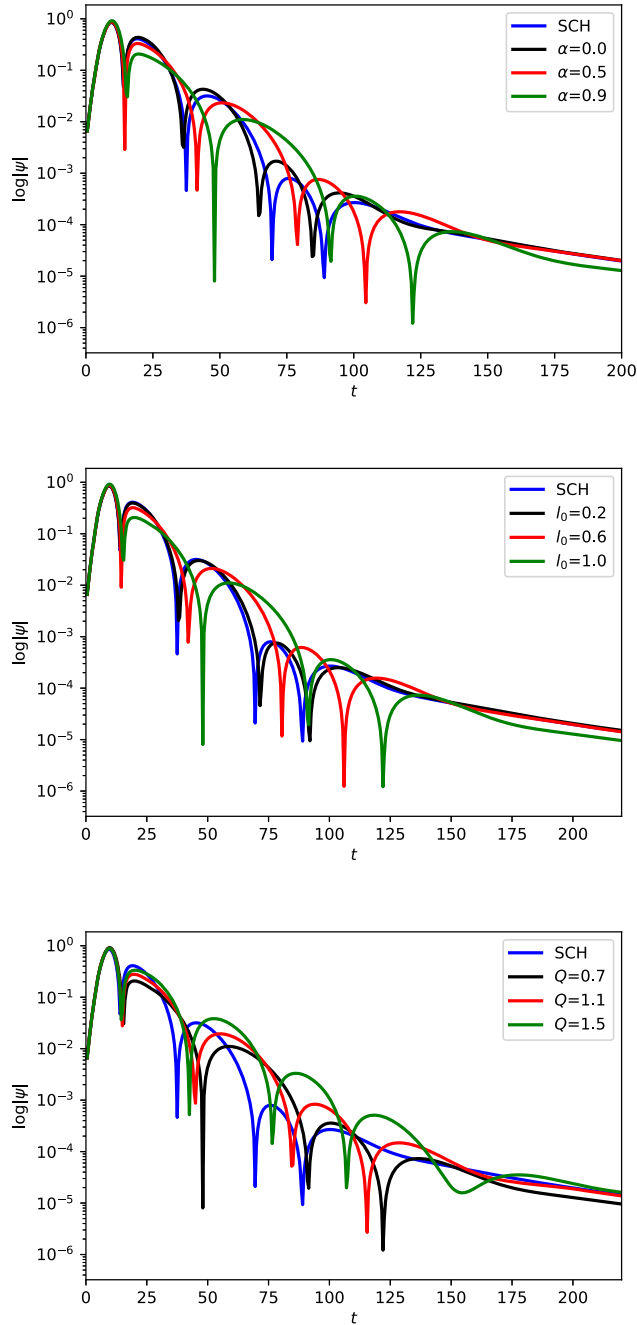


FIG. 1. Time-domain profiles of the scalar field perturbation in the hairy black hole for different α with $M = 1, l = 0, l_0 = 1, Q = 0.7$, for different l_0 with $M = 1, l = 0, \alpha = 0.9, Q = 0.7$, and for different Q with $M = 1, l = 0, l_0 = 1, \alpha = 0.9$, respectively. The blue line represents the TDP of the Schwarzschild black hole (SCH) under scalar field perturbation with $M = 1, l = 0$.

$M = 1, \alpha = 0.9, l_0 = 1$. Our results show that when Q is larger, its TDP decays more slowly. Moreover, in these two figures one can find the clear power-law tail.

In Fig. 3, the TDP of the electromagnetic field in the hairy black hole is given. From Fig. 3, we find that larger α, l_0 and Q make the TDP decay more slowly.

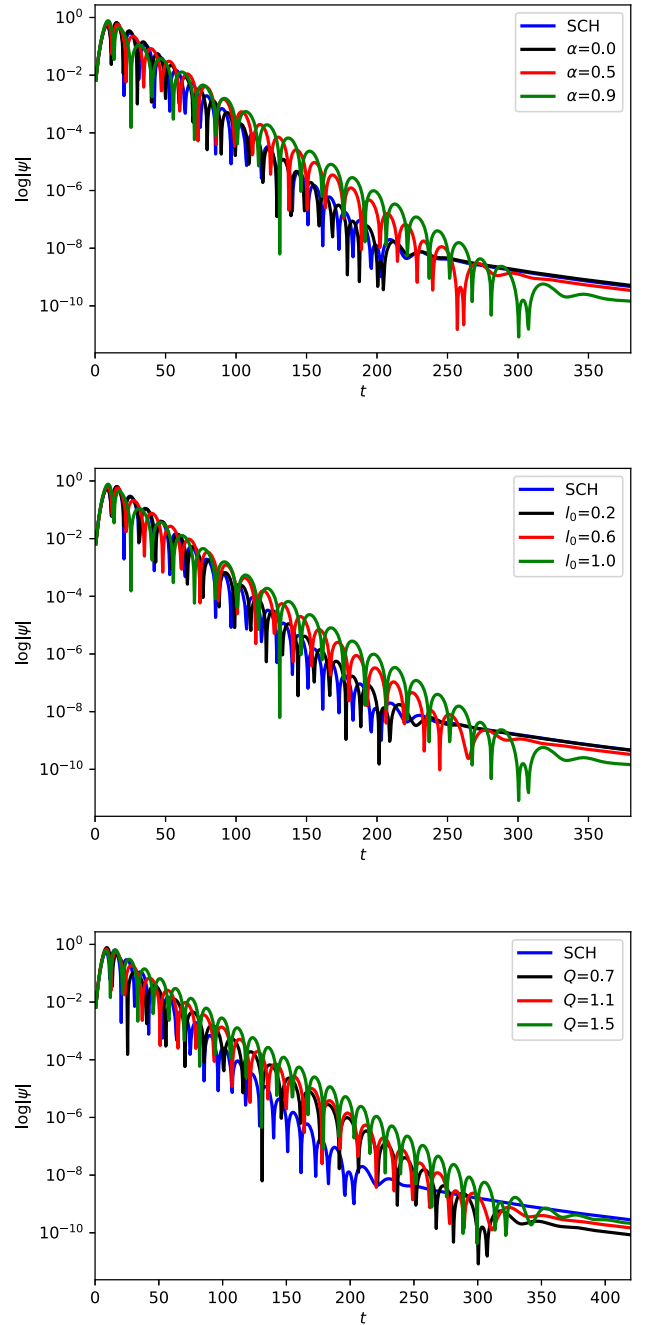


FIG. 2. Time-domain profiles of the scalar field perturbation in the hairy black hole for different α with $M = 1, l = 1, l_0 = 1, Q = 0.7$, for different l_0 with $M = 1, l = 1, \alpha = 0.9, Q = 0.7$, and for different Q with $M = 1, l = 1, l_0 = 1, \alpha = 0.9$, respectively. The blue line represents the TDP of the Schwarzschild black hole (SCH) under scalar field perturbation with $M = 1, l = 1$.

The contributions of these parameters are similar to those of the scalar field perturbation, which demonstrates that an electromagnetic field perturbation and a scalar field perturbation make the TDP of a hairy black hole exhibit similar behavior.

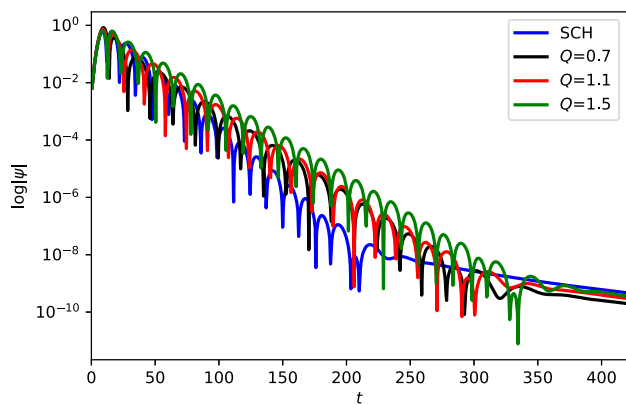
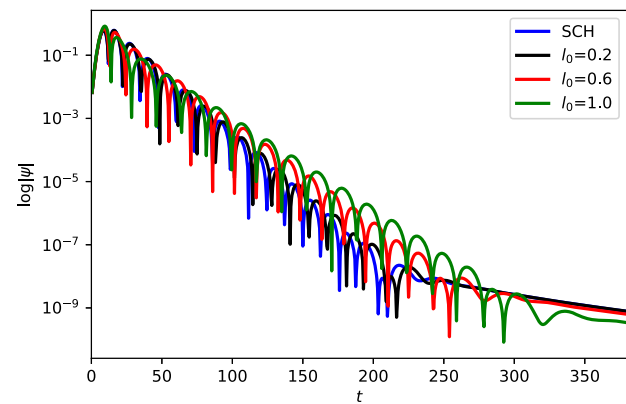
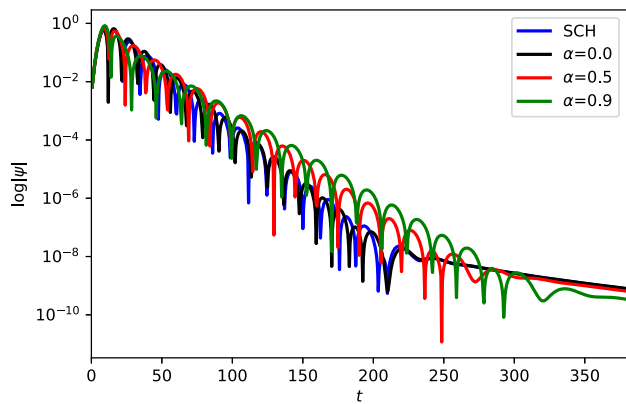


FIG. 3. Time-domain profiles of the electromagnetic field perturbation in the hairy black hole for different α with $M = 1$, $l = 1$, $l_0 = 1$, $Q = 0.7$, for different l_0 with $M = 1$, $l = 1$, $\alpha = 0.9$, $Q = 0.7$, and for different Q with $M = 1$, $l = 1$, $l_0 = 1$, $\alpha = 0.9$, respectively. The blue line represents the TDP of the Schwarzschild black hole (SCH) under electromagnetic field perturbation with $M = 1$, $l = 1$.

In Fig. 4, we present the TDP of the gravitational perturbation in the hairy black hole. The influence of α , l_0 and charge Q on the hairy black hole are studied respectively. We can see that the effects of α , l_0 and Q on the hairy black hole under the gravitational perturbation

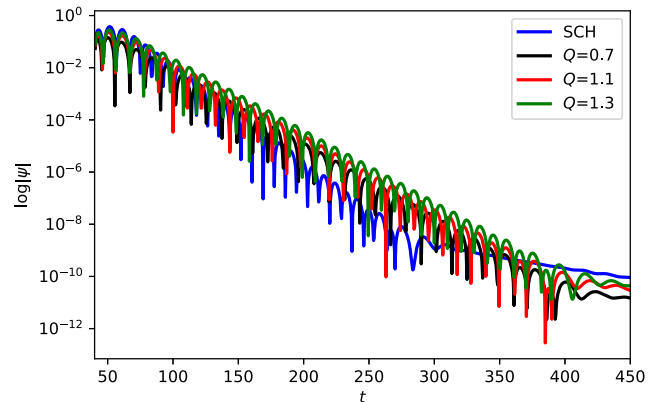
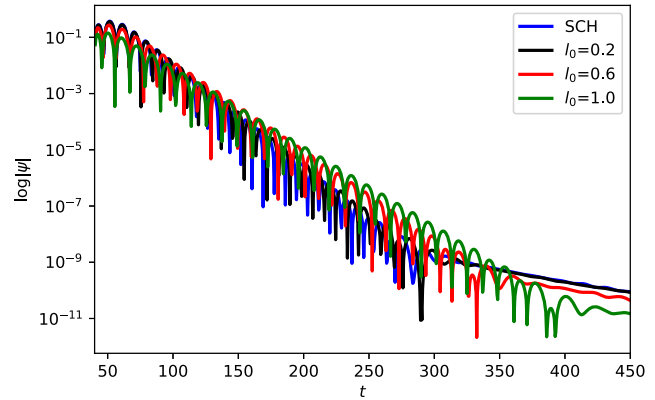
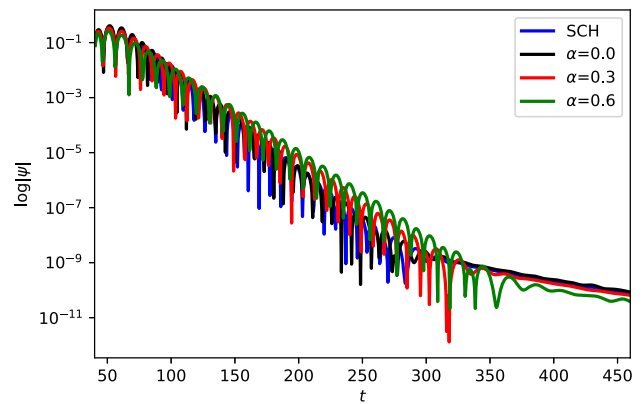


FIG. 4. Time-domain profiles of the gravitational perturbation in the hairy black hole for different α with $M = 1$, $l = 2$, $l_0 = 1$, $Q = 0.7$, for different l_0 with $M = 1$, $l = 2$, $l_0 = 1$, $\alpha = 0.9$, $Q = 0.7$, and for different Q with $M = 1$, $l = 2$, $l_0 = 1$, $\alpha = 0.9$, respectively. The blue line represents the TDP of the Schwarzschild black hole (SCH) under scalar field perturbation with $M = 1$, $l = 2$.

are similar to the scalar field perturbation and the electromagnetic field perturbation.

Apart from studying the time-domain profile, we also study the QNM frequency. Through continuous development, many methods have been proposed to calculate the QNM frequency. The Pöschl-Teller potential approximation method [96,97] is an earlier method for calculating the

TABLE I. QNM frequencies of the scalar field perturbation for a hairy black hole.

$M = 1, l = 1, l_0 = 1, Q = 0.7$			
α	Prony method ($M\omega$)	Sixth-order WKB ($M\omega$)	13th-order WKB ($M\omega$)
0.0	0.321507 – 0.101701 <i>i</i>	0.322775 – 0.0994117 <i>i</i>	0.322772 – 0.0993483 <i>i</i>
0.1	0.300244 – 0.0964229 <i>i</i>	0.303041 – 0.0951931 <i>i</i>	0.303039 – 0.0951213 <i>i</i>
0.2	0.282813 – 0.091302 <i>i</i>	0.286089 – 0.091189 <i>i</i>	0.286092 – 0.0911003 <i>i</i>
0.3	0.268623 – 0.0878727 <i>i</i>	0.271271 – 0.0874315 <i>i</i>	0.27128 – 0.0873223 <i>i</i>
0.4	0.255067 – 0.0820306 <i>i</i>	0.258144 – 0.0839217 <i>i</i>	0.258165 – 0.0837874 <i>i</i>
0.5	0.243646 – 0.0790852 <i>i</i>	0.246392 – 0.0806478 <i>i</i>	0.246423 – 0.0804828 <i>i</i>
0.6	0.233439 – 0.0769056 <i>i</i>	0.23578 – 0.0775934 <i>i</i>	0.235838 – 0.0773884 <i>i</i>
0.7	0.224392 – 0.0749798 <i>i</i>	0.226129 – 0.0747407 <i>i</i>	0.226207 – 0.0744979 <i>i</i>
0.8	0.217691 – 0.0723938 <i>i</i>	0.217300 – 0.072072 <i>i</i>	0.217378 – 0.0718025 <i>i</i>
0.9	0.209181 – 0.0695709 <i>i</i>	0.209181 – 0.0695709 <i>i</i>	0.209304 – 0.0692642 <i>i</i>
$M = 1, l = 1, \alpha = 0.9, Q = 0.7$			
l_0	Prony method ($M\omega$)	Sixth-order WKB ($M\omega$)	13th-order WKB ($M\omega$)
0.2	0.281022 – 0.0955926 <i>i</i>	0.283488 – 0.0947429 <i>i</i>	0.283471 – 0.0945504 <i>i</i>
0.3	0.269242 – 0.0913397 <i>i</i>	0.27147 – 0.0906598 <i>i</i>	0.271478 – 0.0904487 <i>i</i>
0.4	0.258385 – 0.0874759 <i>i</i>	0.260416 – 0.0869074 <i>i</i>	0.260451 – 0.0866649 <i>i</i>
0.5	0.24837 – 0.0839461 <i>i</i>	0.250217 – 0.0834488 <i>i</i>	0.250271 – 0.083192 <i>i</i>
0.6	0.239092 – 0.0807142 <i>i</i>	0.240779 – 0.0802517 <i>i</i>	0.240844 – 0.0799829 <i>i</i>
0.7	0.23046 – 0.0777224 <i>i</i>	0.232021 – 0.0772882 <i>i</i>	0.232096 – 0.0769971 <i>i</i>
0.8	0.222408 – 0.0749569 <i>i</i>	0.223874 – 0.0745339 <i>i</i>	0.223966 – 0.074229 <i>i</i>
0.9	0.214889 – 0.0723729 <i>i</i>	0.216278 – 0.0719677 <i>i</i>	0.216403 – 0.071666 <i>i</i>
1.0	0.209181 – 0.0695709 <i>i</i>	0.209181 – 0.0695709 <i>i</i>	0.209304 – 0.0692642 <i>i</i>
$M = 1, l = 1, l_0 = 1, \alpha = 0.9$			
Q	Prony method ($M\omega$)	Sixth-order WKB ($M\omega$)	13th-order WKB ($M\omega$)
0.7	0.209181 – 0.0695709 <i>i</i>	0.209181 – 0.0695709 <i>i</i>	0.209304 – 0.0692642 <i>i</i>
0.8	0.21196 – 0.0707743 <i>i</i>	0.212052 – 0.0698582 <i>i</i>	0.212157 – 0.069565 <i>i</i>
0.9	0.214681 – 0.0711001 <i>i</i>	0.21552 – 0.0701646 <i>i</i>	0.215628 – 0.0699185 <i>i</i>
1.0	0.218256 – 0.0709727 <i>i</i>	0.219709 – 0.0704705 <i>i</i>	0.219804 – 0.0702317 <i>i</i>
1.1	0.222866 – 0.0706441 <i>i</i>	0.224788 – 0.0707406 <i>i</i>	0.224854 – 0.0705321 <i>i</i>
1.2	0.228786 – 0.0700971 <i>i</i>	0.231015 – 0.0709032 <i>i</i>	0.231059 – 0.070716 <i>i</i>
1.3	0.23683 – 0.0712016 <i>i</i>	0.238783 – 0.0708064 <i>i</i>	0.238807 – 0.070646 <i>i</i>
1.4	0.246787 – 0.0708725 <i>i</i>	0.248804 – 0.070053 <i>i</i>	0.248757 – 0.0699446 <i>i</i>
1.5	0.262831 – 0.0696549 <i>i</i>	0.262188 – 0.0674775 <i>i</i>	0.261999 – 0.0674607 <i>i</i>

black hole’s QNM frequency, but only when the effective potential of the black hole is similar to the Pöschl-Teller potential can a more accurate result be obtained. In Ref. [85], the authors used this method to calculate the QNM frequencies of a hairy black hole under scalar perturbation. In Refs. [69,98], Konoplya used the sixth-order WKB method to study the scattering problem. In Ref. [99], the 13th-order WKB method was presented by using the Padé approximation. In our work, we use the WKB method [77,100–102] and the Prony method to study the QNM frequencies of a hairy black hole caused by gravitational decoupling. The Prony method extracts the QNM frequency from the time-domain profiles by the damped exponents [30,103]

$$\phi(t) \simeq \sum_{i=1}^p C_i e^{-i\omega_i t}. \quad (30)$$

We compare the QNM frequencies extracted from the time-domain profiles using the Prony method with the results calculated by the higher-order WKB method to verify the correctness of time-domain profiles. We list the values of the QNM frequencies in Tables I–IV.

The QNM frequencies of a scalar field perturbation for a hairy black hole are presented in Table I. We study three cases in Table I: in the first one we fix the other parameters ($M = 1, l = 1, l_0 = 1, Q = 0.7$) to study the effect of α on the QNM frequencies of a hairy black hole; in the second

TABLE II. QNM frequencies of the electromagnetic field perturbation for a hairy black hole.

$M = 1, l = 1, l_0 = 1, Q = 0.7$			
α	Prony method ($M\omega$)	Sixth-order WKB ($M\omega$)	13th-order WKB ($M\omega$)
0.0	0.27438 - 0.0952652i	0.277264 - 0.0951071i	0.277328 - 0.0948974i
0.1	0.257552 - 0.0915071i	0.259522 - 0.0909144i	0.259592 - 0.0907009i
0.2	0.242204 - 0.0868901i	0.244445 - 0.0869722i	0.244524 - 0.0867263i
0.3	0.229607 - 0.0834999i	0.231379 - 0.0832965i	0.231462 - 0.0830699i
0.4	0.218479 - 0.0802702i	0.21989 - 0.0798778i	0.219977 - 0.0796442i
0.5	0.208539 - 0.0771759i	0.209666 - 0.0766987i	0.20978 - 0.0764508i
0.6	0.199608 - 0.0742378i	0.200482 - 0.0737389i	0.200604 - 0.0734884i
0.7	0.191541 - 0.0714914i	0.192165 - 0.0709789i	0.192297 - 0.0707073i
0.8	0.184193 - 0.0689691i	0.184584 - 0.0684005i	0.184723 - 0.0681492i
0.9	0.177388 - 0.0672283i	0.177635 - 0.0659867i	0.17778 - 0.0657295i
$M = 1, l = 1, \alpha = 0.9, Q = 0.7$			
l_0	Prony method ($M\omega$)	Sixth-order WKB ($M\omega$)	13th-order WKB ($M\omega$)
0.2	0.238957 - 0.0903121i	0.240451 - 0.0899668i	0.240592 - 0.0895844i
0.3	0.228902 - 0.086411i	0.230301 - 0.086083i	0.230435 - 0.0857165i
0.4	0.219661 - 0.0827886i	0.220963 - 0.0825113i	0.221115 - 0.082122i
0.5	0.211118 - 0.0794722i	0.212344 - 0.0792167i	0.212507 - 0.0788714i
0.6	0.203217 - 0.0763974i	0.204367 - 0.0761695i	0.204528 - 0.075829i
0.7	0.195489 - 0.0730517i	0.196962 - 0.0733442i	0.197118 - 0.0730409i
0.8	0.189112 - 0.0709165i	0.190071 - 0.070718i	0.190225 - 0.0704139i
0.9	0.182467 - 0.0680648i	0.183643 - 0.0682712i	0.183795 - 0.0679941i
1.0	0.177388 - 0.0672283i	0.177635 - 0.0659867i	0.17778 - 0.0657295i
$M = 1, l = 1, l_0 = 1, \alpha = 0.9$			
Q	Prony method ($M\omega$)	Sixth-order WKB ($M\omega$)	13th-order WKB ($M\omega$)
0.7	0.177388 - 0.0672283i	0.177635 - 0.0659867i	0.17778 - 0.0657295i
0.8	0.179783 - 0.0668075i	0.180372 - 0.0663587i	0.180517 - 0.066101i
0.9	0.18274 - 0.0668985i	0.183697 - 0.0667678i	0.183843 - 0.066497i
1.0	0.186791 - 0.0674179i	0.18774 - 0.0671974i	0.187859 - 0.066929i
1.1	0.191665 - 0.067882i	0.192683 - 0.0676172i	0.192789 - 0.0673285i
1.2	0.197621 - 0.0682103i	0.198814 - 0.0679582i	0.198927 - 0.0676624i
1.3	0.205651 - 0.0687884i	0.206573 - 0.0680707i	0.206693 - 0.0677617i
1.4	0.216046 - 0.0686647i	0.216777 - 0.0675363i	0.216889 - 0.0672306i
1.5	0.229584 - 0.0662932i	0.230929 - 0.0649291i	0.230986 - 0.0646869i

one we specify other parameters ($M = 1, l = 1, \alpha = 0.9, Q = 0.7$) to research the impact of l_0 on the QNM frequencies of a hairy black hole; and in the third one we fix the other parameters ($M = 1, l = 1, l_0 = 1, \alpha = 0.9$) to investigate the effect of Q on the QNM frequencies of a hairy black hole. One can see that there is only a slight deviation between the QNM frequency extracted using the TDP and the result from the high-order WKB method in the three cases, which is enough to prove the accuracy of the TDP. It is seen that when α increases, the real part and imaginary part of the QNM frequency are both smaller, that is, the oscillation frequency of GWs is decreasing and the damping is also decreasing. In addition, when l_0 increases, we can also find that the real and imaginary parts of the QNM frequency are decreasing. The decrease of the imaginary part indicates that its decay slows down, which

is consistent with the results shown in Fig. 2. However, we find that the same trend for different α and l_0 does not continue to the results for various charges Q . The increase of charge Q under the scalar perturbation leads to the real part of the QNM frequencies increasing, whereas the imaginary part decreases, which demonstrates that the oscillation frequency of GWs is increasing, and the decay rate is slower. This is the reason why the power-law tails appear early in Fig. 2 when the charge Q is small, and this behavior is similar to the results of different α and l_0 , i.e. smaller α and l_0 correspond to earlier power-law tails.

In Table II, the QNM frequencies of the electromagnetic field perturbation for a hairy black hole are given. For different α , the parameter settings are $M = 1, l = 1, l_0 = 1, Q = 0.7$. For different l_0 , the parameter settings are $M = 1, l = 1, \alpha = 0.9, Q = 0.7$. For different Q , the parameter

TABLE III. QNM frequencies of the gravitational perturbation for a hairy black hole.

$M = 1, l = 2, l_0 = 1, Q = 0.7$			
α	Prony method ($M\omega$)	Sixth-order WKB ($M\omega$)	13th-order WKB ($M\omega$)
0.0	0.421319 - 0.093321 <i>i</i>	0.41962 - 0.0910065 <i>i</i>	0.419637 - 0.0909727 <i>i</i>
0.1	0.394301 - 0.0872158 <i>i</i>	0.392428 - 0.087046 <i>i</i>	0.392426 - 0.0870356 <i>i</i>
0.2	0.369882 - 0.085768 <i>i</i>	0.369425 - 0.0833178 <i>i</i>	0.369409 - 0.0833276 <i>i</i>
0.3	0.350611 - 0.0815108 <i>i</i>	0.349553 - 0.0798375 <i>i</i>	0.349535 - 0.079867 <i>i</i>
0.4	0.332492 - 0.0763707 <i>i</i>	0.332112 - 0.0765966 <i>i</i>	0.332093 - 0.0766124 <i>i</i>
0.5	0.315724 - 0.0736334 <i>i</i>	0.316614 - 0.0735789 <i>i</i>	0.316588 - 0.0736032 <i>i</i>
0.6	0.303406 - 0.0710666 <i>i</i>	0.302703 - 0.0707663 <i>i</i>	0.30268 - 0.0707763 <i>i</i>
0.7	0.290561 - 0.0682911 <i>i</i>	0.290115 - 0.0681411 <i>i</i>	0.290095 - 0.0681618 <i>i</i>
0.8	0.278566 - 0.066302 <i>i</i>	0.278644 - 0.0656872 <i>i</i>	0.27864 - 0.0657188 <i>i</i>
0.9	0.266795 - 0.0643959 <i>i</i>	0.26813 - 0.0633896 <i>i</i>	0.268131 - 0.0634126 <i>i</i>
$M = 1, l = 2, \alpha = 0.9, Q = 0.7$			
l_0	Prony method ($M\omega$)	Sixth-order WKB ($M\omega$)	13th-order WKB ($M\omega$)
0.2	0.364607 - 0.0865609 <i>i</i>	0.363216 - 0.0864224 <i>i</i>	0.363004 - 0.0863902 <i>i</i>
0.3	0.346775 - 0.0833835 <i>i</i>	0.347865 - 0.08270 <i>i</i>	0.347729 - 0.0827333 <i>i</i>
0.4	0.333299 - 0.0791465 <i>i</i>	0.333738 - 0.0792706 <i>i</i>	0.333645 - 0.0793122 <i>i</i>
0.5	0.320798 - 0.0759211 <i>i</i>	0.320696 - 0.0761044 <i>i</i>	0.320636 - 0.0761492 <i>i</i>
0.6	0.309047 - 0.0731385 <i>i</i>	0.30862 - 0.0731748 <i>i</i>	0.308578 - 0.0732138 <i>i</i>
0.7	0.298027 - 0.0706296 <i>i</i>	0.297408 - 0.0704583 <i>i</i>	0.29738 - 0.0704918 <i>i</i>
0.8	0.287702 - 0.0683308 <i>i</i>	0.286972 - 0.0679339 <i>i</i>	0.286956 - 0.0679646 <i>i</i>
0.9	0.278041 - 0.0662711 <i>i</i>	0.277235 - 0.0655832 <i>i</i>	0.277228 - 0.0656096 <i>i</i>
1.0	0.266795 - 0.0643959 <i>i</i>	0.26813 - 0.0633896 <i>i</i>	0.268131 - 0.0634126 <i>i</i>
$M = 1, l = 2, l_0 = 1, \alpha = 0.9$			
Q	Prony method ($M\omega$)	Sixth-order WKB ($M\omega$)	13th-order WKB ($M\omega$)
0.7	0.266795 - 0.0643959 <i>i</i>	0.26813 - 0.0633896 <i>i</i>	0.268131 - 0.0634126 <i>i</i>
0.8	0.271865 - 0.0645973 <i>i</i>	0.272466 - 0.0637162 <i>i</i>	0.272459 - 0.0637328 <i>i</i>
0.9	0.278479 - 0.0651984 <i>i</i>	0.277738 - 0.0640789 <i>i</i>	0.27774 - 0.0640953 <i>i</i>
1.0	0.284881 - 0.0651774 <i>i</i>	0.284153 - 0.0644651 <i>i</i>	0.284135 - 0.0644731 <i>i</i>
1.1	0.292663 - 0.0653426 <i>i</i>	0.292016 - 0.0648472 <i>i</i>	0.292003 - 0.0648387 <i>i</i>
1.2	0.302629 - 0.0659483 <i>i</i>	0.301795 - 0.065162 <i>i</i>	0.301803 - 0.0651248 <i>i</i>
1.3	0.315112 - 0.0655522 <i>i</i>	0.314282 - 0.0652534 <i>i</i>	0.314329 - 0.0651797 <i>i</i>
1.4	0.33039 - 0.0639798 <i>i</i>	0.330944 - 0.0646919 <i>i</i>	0.331053 - 0.0645997 <i>i</i>
1.5	0.354654 - 0.0600052 <i>i</i>	0.355086 - 0.0619111 <i>i</i>	0.355174 - 0.0618972 <i>i</i>

settings are $M = 1, l = 1, l_0 = 1, \alpha = 0.9$. In addition, we also give the QNM frequencies of a hairy black hole under gravitational perturbation in Table III. We can see that Table II and Table III present the same trend as in Table I for different cases, which further demonstrates that scalar field perturbation, electromagnetic perturbation and gravitational perturbation have similar qualitative behavior to the hairy black hole caused by gravitational decoupling. In particular, the effects of α and l_0 on the real part of the QNM are opposite to that of Q , i.e., an increase in α and l_0 will decrease the oscillation frequency of gravitational waves, whereas an increase in Q will increase the oscillation frequency of gravitational waves.

Table IV shows the QNM frequencies of scalar field, electromagnetic field, and gravitational perturbations with

different l . It is interesting to note that the increase of the multipole moment l will significantly increase the oscillation frequency of gravitational waves, whereas the effect on the decay rate is very small. The most important point in Table IV is that when $\alpha = 0, Q = 0$, our results can reproduce the results of the Schwarzschild black hole very well. Moreover, in Table IV, we calculate the error of the 13th-order WKB method. One can find that the error of the 13th-order WKB method for a small l will be larger than that of the large l , and the error of scalar field perturbation is larger than that of electromagnetic field and gravitational perturbations. For example, for the gravitational perturbation results in Table IV, when $l = 2$, the error is about 4.47532×10^{-5} , and it is about 1.03191×10^{-8} for $l = 4$. On the other hand, Table V gives the deviation of the QNM

TABLE IV. QNM frequencies of scalar field (Scal), electromagnetic field (Elec), and gravitational (Grav) perturbations for different l .

$M = 1, \alpha = 0, Q = 0$					
Field	l	Prony method ($M\omega$)	Sixth-order WKB ($M\omega$)	13th-order WKB ($M\omega$)	Error
Scal	0	$0.105932 - 0.103975i$	$0.110493 - 0.100793i$	$0.111336 - 0.103793i$	2.57859×10^{-3}
	1	$0.289254 - 0.0967834i$	$0.29291 - 0.0977616i$	$0.292935 - 0.0976625i$	5.63328×10^{-6}
	2	$0.476682 - 0.0964193i$	$0.483642 - 0.0967661i$	$0.483643 - 0.0967596i$	3.07067×10^{-7}
Elec	1	$0.245525 - 0.0912522i$	$0.248191 - 0.092637i$	$0.24826 - 0.0924874i$	1.65754×10^{-5}
	2	$0.451157 - 0.0927749i$	$0.457593 - 0.095011i$	$0.457595 - 0.0950047i$	4.82647×10^{-7}
	3	$0.644805 - 0.0930214i$	$0.656898 - 0.0956171i$	$0.656899 - 0.0956163i$	4.67008×10^{-7}
Grav	2	$0.369919 - 0.0893064i$	$0.373619 - 0.088891i$	$0.373583 - 0.0889827i$	8.39293×10^{-5}
	3	$0.590055 - 0.0919906i$	$0.599443 - 0.0927025i$	$0.599443 - 0.0927028i$	1.79319×10^{-8}
	4	$0.792386 - 0.094910i$	$0.809178 - 0.0941641i$	$0.809178 - 0.094164i$	3.42659×10^{-8}

$M = 1, l_0 = 1, \alpha = 0.9, Q = 0.7$					
Field	l	Prony method ($M\omega$)	Sixth-order WKB ($M\omega$)	13th-order WKB ($M\omega$)	Error
Scal	0	$0.0757766 - 0.0719676i$	$0.0850839 - 0.064694i$	$0.0840857 - 0.0674921i$	4.27326×10^{-3}
	1	$0.209635 - 0.0696289i$	$0.209181 - 0.0695709i$	$0.209304 - 0.0692642i$	1.35598×10^{-5}
	2	$0.345137 - 0.0681247i$	$0.345759 - 0.0687022i$	$0.345765 - 0.0686858i$	4.57878×10^{-7}
Elec	1	$0.177388 - 0.0672283i$	$0.177635 - 0.0659867i$	$0.17778 - 0.0657295i$	1.51868×10^{-5}
	2	$0.325863 - 0.0671239i$	$0.327385 - 0.0675054i$	$0.327391 - 0.0674944i$	1.26352×10^{-6}
	3	$0.466492 - 0.0689451i$	$0.469885 - 0.0679249i$	$0.469885 - 0.0679233i$	1.61534×10^{-7}
Grav	2	$0.266795 - 0.0643959i$	$0.26813 - 0.0633896i$	$0.268131 - 0.0634126i$	4.47532×10^{-5}
	3	$0.425910 - 0.066640i$	$0.429374 - 0.0659638i$	$0.429374 - 0.0659635i$	7.92364×10^{-8}
	4	$0.580939 - 0.067654i$	$0.579217 - 0.0669528i$	$0.579217 - 0.0669526i$	1.03191×10^{-8}

 TABLE V. Deviation of the QNM frequencies of Schwarzschild black hole ($M = 1, \alpha = 0, Q = 0$) calculated by the Prony method relative to Iyer's results.

Field	l	Prony method ($M\omega$)	Iyer's results [104] ($M\omega$)	Frequency deviations	Decay rate deviations
Scal	0	$0.103129 - 0.107250i$	$0.1046 - 0.1152i$	1.4%	6.9%
	1	$0.289254 - 0.0967834i$	$0.2911 - 0.0980i$	0.6%	1.2%
	2	$0.476682 - 0.0964193i$	$0.4832 - 0.0968i$	1.3%	0.4%
Elec	1	$0.245525 - 0.0912522i$	$0.2459 - 0.0931i$	0.2%	2.0%
	2	$0.451157 - 0.0927749i$	$0.4571 - 0.0951i$	1.3%	2.4%
	3	$0.644805 - 0.0930214i$	$0.6567 - 0.0956i$	1.8%	2.7%
Grav	2	$0.369919 - 0.0893064i$	$0.3732 - 0.0892i$	0.9%	0.1%
	3	$0.590055 - 0.0919906i$	$0.5993 - 0.0927i$	1.5%	0.7%
	4	$0.792386 - 0.094910i$	$0.8091 - 0.0942i$	2.0%	0.8%

frequencies of a Schwarzschild black hole ($M = 1, \alpha = 0, Q = 0$) calculated using the Prony method relative to Iyer's results [104]. We can see that for the scalar field perturbation $l = 0$, the deviation of the decay rate reaches 6.9%, and for other cases, whether it is for the frequency or decay rate, the deviation does not exceed 2.7%. The reason for the large deviation of the scalar field perturbation $l = 0$ may be found in Fig. 1. We can see that the duration of the ringdown of the

TDP is very short from Fig. 1, which implies that the Prony method is not particularly accurate in this case. In Table VI, the behaviors of the real parts and imaginary parts of QNM frequencies for a hairy black hole under gravitational perturbation with different overtone numbers are shown. We observe that the real parts of QNM frequencies decrease with the overtone number, and the imaginary parts of QNM frequencies increase with the overtone number.

TABLE VI. QNM frequencies of a hairy black hole for gravitational perturbations with different overtone numbers.

$\alpha = 0.01, Q = 0.075, l_0 = 0.15$								
l	n	$(M\omega_n)$	l	n	$(M\omega_n)$	l	n	$(M\omega_n)$
2	0	$0.37357 - 0.0889782i$	3	0	$0.599413 - 0.0926969i$	4	0	$0.809134 - 0.0941578i$
	1	$0.346071 - 0.273517i$		1	$0.582598 - 0.281333i$		1	$0.796583 - 0.284316i$
	2	$0.298458 - 0.477529i$		2	$0.551573 - 0.479015i$		2	$0.772649 - 0.479881i$
	3	$0.248739 - 0.708946i$		3	$0.511842 - 0.690648i$		3	$0.739752 - 0.683955i$

IV. BOUNDING THE GREYBODY FACTORS AND HIGH-ENERGY ABSORPTION CROSS SECTION VIA THE SINC APPROXIMATION

A. Bounding the greybody factor

In this section, the lower bound of the greybody factor of a hairy black hole is investigated. There are many methods to calculate the lower bound, and the WKB method is the most frequently used one [105,106]. In Ref. [98], Konoplya *et al.* studied the greybody factor of a wormhole using the sixth-order WKB method. In Ref. [107], they investigated the greybody factor of a Bardeen–de Sitter black hole under gravitational perturbation and electromagnetic perturbation using the WKB method. We use another rigorous method to calculate the greybody. In this method, the general bound of the greybody for a black hole is written as [78–80,108–114]

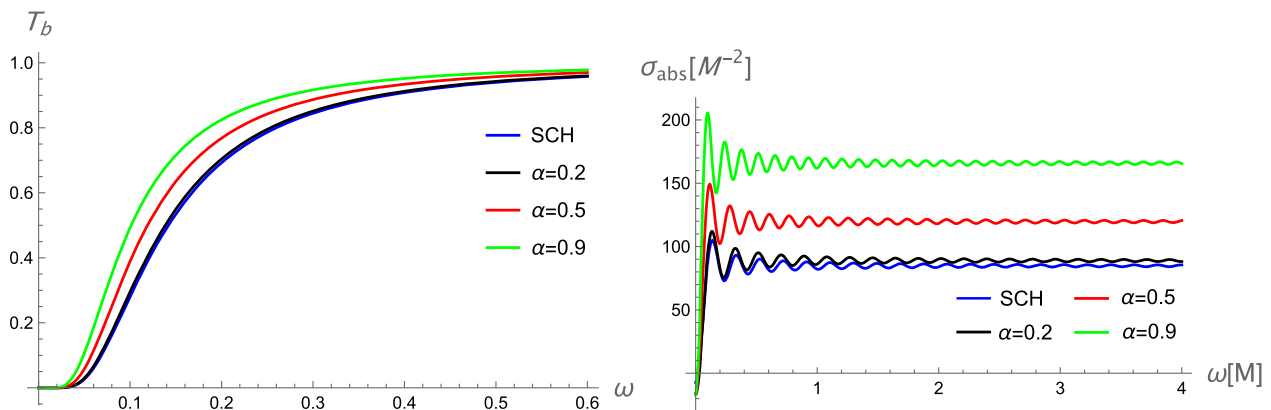
$$T_b \geq \text{sech}^2\left(\frac{1}{2\omega} \int_{-\infty}^{\infty} |V| \frac{dr}{f(r)}\right). \quad (31)$$

Then one can use the Regge-Wheeler potential from Sec. II, and numerically plot the variation of the greybody factor with various parameters (α , l_0 and Q), as seen in Figs. 5, 6 and 7. From these figures, we can see that the value of the greybody bound is zero when the frequency is

minimal, and the value of the greybody bound is 1 when the frequency is large enough. This shows that when the frequency is small, the wave is basically totally reflected. As the frequency increases, a part of the wave can pass through the potential barrier due to the tunneling effect. When the frequency reaches a certain critical value, the wave will not be reflected. In addition, one can see that for larger α and l_0 , the greybody bound is also larger, whereas the effect of the hair Q is opposite. Therefore, for the hairy black hole spacetime with large charge Q , the hairy black hole greatly scatters the incident wave. On the other hand, the greybody factors for Schwarzschild black holes have been rigorously analyzed [78,115]. Compared with the greybody factors of a Schwarzschild black hole, the greybody factors of a hairy black hole are larger than those of a Schwarzschild black hole when the frequency is fixed, which demonstrates that the probability of Hawking radiation reaching spatial infinity in the hairy black hole spacetime is greater than that in the Schwarzschild black hole spacetime.

B. High-energy absorption cross section with the sinc approximation

The oscillatory pattern of the high-energy absorption cross section corresponding to a sinc(x) function within the photon sphere [with sinc(x) denoting $\sin c(x) \equiv \sin(x)/x$].


 FIG. 5. Greybody bound (left panel) T_b as a function of ω , and the total absorption cross section (right panel) for different values of α , with $M = 1, l_0 = 1, Q = 0.7$.

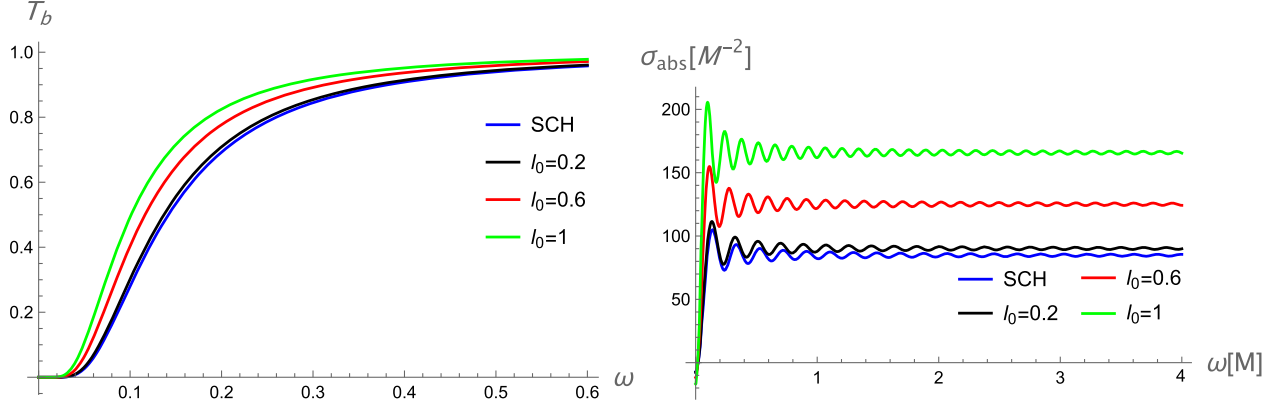


FIG. 6. Greybody bound (left panel) T_b as a function of ω , and the total absorption cross section (right panel) for different values of l_0 , with $M = 1, \alpha = 0.9, Q = 0.7$.

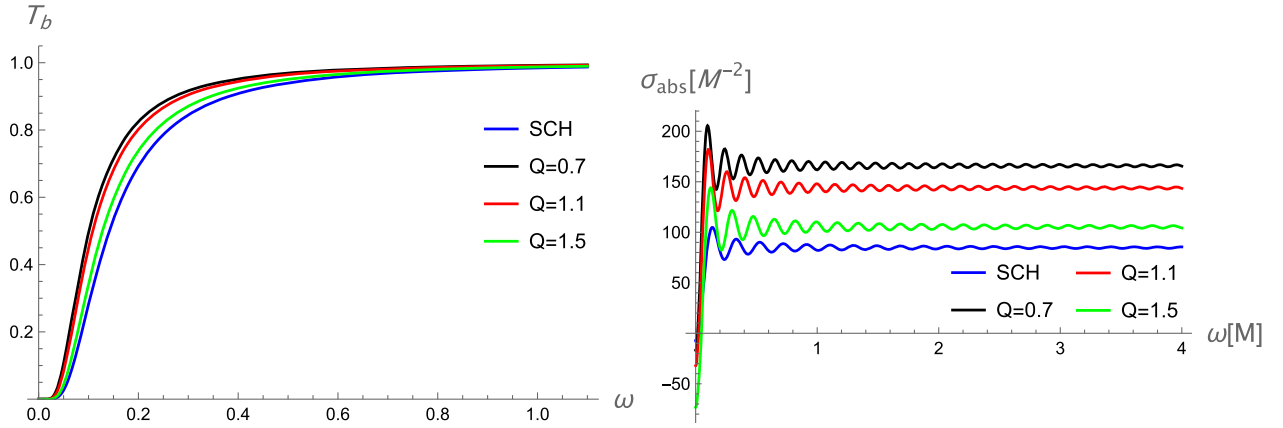


FIG. 7. Greybody bound (left panel) T_b as a function of ω , and the total absorption cross section (right panel) for different values of the charge Q , with $M = 1, \alpha = 0.9, l_0 = 1$.

The oscillatory part of the absorption cross section in the eikonal limit is [84]

$$\sigma_{\text{osc}}(\omega) = -8\pi\sigma_{\text{geo}}n_c e^{-\pi n_c} \sin c[2\pi b_c \omega] \quad (32)$$

where

$$n_c = \sqrt{f(r_c) - \frac{r_c^2}{2} f''(r_c)}, \quad (33)$$

and the eikonal cross section is $\sigma_{\text{geo}} = \pi b_c^2$ with the critical impact parameter $b_c = \frac{r_c}{\sqrt{f(r_c)}}$.

Then the sinc approximation states that the total absorption cross section at the eikonal limit is $\sigma_{\text{abs}} \approx \sigma_{\text{osc}} + \sigma_{\text{geo}}$ [81,84,116–118]. In Figs. 5, 6 and 7 we plot the total absorption cross section for various values of α , l_0 and Q . One can find that the total absorption cross section seems to be divided into three phases with the increase of ω : first, the fast growing phase, then the oscillations phase, and finally the stabilization around a certain value. Moreover, we find that the hairy black hole has a larger absorption cross

section when α and l_0 are larger, and the absorption cross section of the hairy black hole is smaller when the charge Q is larger. Compared with the total absorption cross section of Schwarzschild black holes, our results show that the total absorption cross section of Schwarzschild black holes is always smaller than that of hairy black holes.

V. CONCLUSION

In summary, we studied the QNM of hairy black holes caused by gravitational decoupling. By studying the scalar field, electromagnetic field, and axial gravitational perturbations, the time-domain profiles of QNMs were given, and the QNM frequencies of hairy black holes were fitted according to the time-domain profiles, which are consistent with the results of the high-order WKB method. We conclude that for hairy black holes caused by gravitational decoupling, the effects of these hairs (α , l_0 , Q) on time-domain profiles and QNM frequencies under scalar field, electromagnetic field, and gravitational perturbations show similar behavior, i.e. an increase in α and l_0 decrease the oscillation frequency of the gravitational-wave signal

emitted by a perturbed hairy black hole, and an increase in Q increased the oscillation frequency of the GW signal. In addition, an increase of the multipole moment l obviously increases the oscillation frequency of the gravitational-wave signal, whereas the influence on its decay rate is very small. In the end, we studied the bounding of the greybody factor and absorption cross section of hairy black holes using the sinc approximation. We found that for larger α and l_0 , the greybody bound and absorption cross section are also larger, whereas the contribution of the charge Q is the opposite. Therefore, for the hairy black hole spacetime with large charge Q , the propagating waves can be greatly reflected by the potential barrier. A smaller value of the greybody factor implies that the probability of gravitational radiation reaching spatial infinity is lower. Consequently, an increase in α and l_0 can increase the probability of gravitational radiation arriving at spatial infinity. In addition, the increase of α and l_0 makes the total absorption cross section also increase, whereas the increase of Q makes the total absorption cross section decrease. We expect our results to provide some direction for detecting hairy black holes caused by gravitational decoupling in future experiments. On the other hand, there are some

regions of the parameter space of the hairy black hole we studied, which will make it become a naked singularity. In the future, it will be interesting to probe such regions of the parameter space that may pose a threat to the deterministic nature of gravitational theories with spherically symmetric solutions, and in this way one can understand near-extremal modes and strong cosmic censorship in spherical symmetric black holes [119–127].

ACKNOWLEDGMENTS

We greatly appreciate anonymous referees for constructive comments. We also are very grateful to J. Ovalle and Poulami Dutta Roy for useful correspondences. This research was funded by the National Natural Science Foundation of China (Grants No. 12265007 and 11565009), the Natural Science Special Research Foundation of Guizhou University (Grant No. X2020068), and the Science and Technology Foundation of Guizhou Province (No. ZK[2022]YB029). A. Ö. would like to acknowledge the contribution of the COST Action CA18108—Quantum gravity phenomenology in the multi-messenger approach (QG-MM).

-
- [1] R. Ruffini and J. A. Wheeler, *Phys. Today* **24** No. 1, 30 (1971).
 - [2] S. W. Hawking, *Commun. Math. Phys.* **25**, 152 (1972).
 - [3] S. W. Hawking, M. J. Perry, and A. Strominger, *Phys. Rev. Lett.* **116**, 231301 (2016).
 - [4] D. Grumiller, A. Pérez, M. M. Sheikh-Jabbari, R. Troncoso, and C. Zwikel, *Phys. Rev. Lett.* **124**, 041601 (2020).
 - [5] K. G. Zloshchastiev, *Phys. Rev. Lett.* **94**, 121101 (2005).
 - [6] T. P. Sotiriou and V. Faraoni, *Phys. Rev. Lett.* **108**, 081103 (2012).
 - [7] A. Cisterna and C. Erices, *Phys. Rev. D* **89**, 084038 (2014).
 - [8] G. Antoniou, A. Bakopoulos, and P. Kanti, *Phys. Rev. Lett.* **120**, 131102 (2018).
 - [9] J. Ovalle, *Phys. Rev. D* **95**, 104019 (2017).
 - [10] J. Ovalle, *Phys. Lett. B* **788**, 213 (2019).
 - [11] M. Sharif and S. Sadiq, *Eur. Phys. J. C* **78**, 410 (2018).
 - [12] J. Ovalle, C. Posada, and Z. Stuchlík, *Classical Quantum Gravity* **36**, 205010 (2019).
 - [13] J. Ovalle, R. Casadio, R. da Rocha, A. Sotomayor, and Z. Stuchlík, *Europhys. Lett.* **124**, 20004 (2018).
 - [14] J. Ovalle, R. Casadio, R. da Rocha, and A. Sotomayor, *Eur. Phys. J. C* **78**, 122 (2018).
 - [15] A. Rincón, L. Gabbanelli, E. Contreras, and F. Tello-Ortiz, *Eur. Phys. J. C* **79**, 873 (2019).
 - [16] L. Gabbanelli, A. Rincón, and C. Rubio, *Eur. Phys. J. C* **78**, 370 (2018).
 - [17] E. Contreras, A. Rincón, and P. Bargueño, *Eur. Phys. J. C* **79**, 216 (2019).
 - [18] G. Panotopoulos and A. Rincón, *Eur. Phys. J. C* **78**, 851 (2018).
 - [19] F. Tello-Ortiz, *Eur. Phys. J. C* **80**, 413 (2020).
 - [20] R. Casadio and J. Ovalle, *Phys. Lett. B* **715**, 251 (2012).
 - [21] J. Ovalle and F. Linares, *Phys. Rev. D* **88**, 104026 (2013).
 - [22] J. Ovalle, F. Linares, A. Pasqua, and A. Sotomayor, *Classical Quantum Gravity* **30**, 175019 (2013).
 - [23] J. Ovalle, L. A. Gergely, and R. Casadio, *Classical Quantum Gravity* **32**, 045015 (2015).
 - [24] J. Ovalle, R. Casadio, R. de Rocha, A. Sotomayor, and Z. Stuchlík, *Eur. Phys. J. C* **78**, 960 (2018).
 - [25] J. Ovalle, R. Casadio, E. Contreras, and A. Sotomayor, *Phys. Dark Universe* **31**, 100744 (2021).
 - [26] C. V. Vishveshwara, *Nature (London)* **227**, 936 (1970).
 - [27] K. D. Kokkotas and B. G. Schmidt, *Living Rev. Relativity* **2**, 2 (1999).
 - [28] H.-P. Nollert, *Classical Quantum Gravity* **16**, R159 (1999).
 - [29] V. Cardoso and P. Pani, *Living Rev. Relativity* **22**, 4 (2019).
 - [30] R. A. Konoplya and A. Zhidenko, *Rev. Mod. Phys.* **83**, 793 (2011).
 - [31] C. Chirenti, *Braz. J. Phys.* **48**, 102 (2018).
 - [32] R. C. Pantig, L. Mastroiuto, G. Lambiase, and A. Övgün, *Eur. Phys. J. C* **82**, 1155 (2022).
 - [33] B. P. Abbott *et al.* (LIGO Scientific and Virgo Collaborations), *Phys. Rev. Lett.* **116**, 061102 (2016).
 - [34] M. H.-Y. Cheung, K. Destounis, R. P. Macedo, E. Berti, and V. Cardoso, *Phys. Rev. Lett.* **128**, 111103 (2022).

- [35] V. Boyanov, K. Destounis, R. Panosso Macedo, V. Cardoso, and J. L. Jaramillo, [arXiv:2209.12950](#).
- [36] N. Chatzifotis, C. Vlachos, K. Destounis, and E. Papantonopoulos, *Gen. Relativ. Gravit.* **54**, 49 (2022).
- [37] V. Cardoso, E. Franzin, and P. Pani, *Phys. Rev. Lett.* **116**, 171101 (2016); **117**, 089902(E) (2016).
- [38] V. Cardoso, S. Hopper, C. F. B. Macedo, C. Palenzuela, and P. Pani, *Phys. Rev. D* **94**, 084031 (2016).
- [39] V. Cardoso and P. Pani, *Nat. Astron.* **1**, 586 (2017).
- [40] E. Maggio, A. Testa, S. Bhagwat, and P. Pani, *Phys. Rev. D* **100**, 064056 (2019).
- [41] R. A. Konoplya and A. Zhidenko, *Europhys. Lett.* **138**, 49001 (2022).
- [42] R. A. Konoplya, Z. Stuchlík, and A. Zhidenko, *Phys. Rev. D* **99**, 024007 (2019).
- [43] K. A. Bronnikov and R. A. Konoplya, *Phys. Rev. D* **101**, 064004 (2020).
- [44] M. S. Churilova, R. A. Konoplya, Z. Stuchlik, and A. Zhidenko, *J. Cosmol. Astropart. Phys.* **10** (2021) 010.
- [45] Y. Yang, D. Liu, Z. Xu, Y. Xing, S. Wu, and Z.-W. Long, *Phys. Rev. D* **104**, 104021 (2021).
- [46] M.-Y. Ou, M.-Y. Lai, and H. Huang, *Eur. Phys. J. C* **82**, 452 (2022).
- [47] C. Vlachos, E. Papantonopoulos, and K. Destounis, *Phys. Rev. D* **103**, 044042 (2021).
- [48] L. F. Longo Micchi, N. Afshordi, and C. Chirenti, *Phys. Rev. D* **103**, 044028 (2021).
- [49] A. Chowdhury and N. Banerjee, *Phys. Rev. D* **102**, 124051 (2020).
- [50] G. Guo, P. Wang, H. Wu, and H. Yang, *J. High Energy Phys.* **06** (2022) 073.
- [51] P. Dutta Roy, S. Aneesh, and S. Kar, *Eur. Phys. J. C* **80**, 850 (2020).
- [52] V. Ferrari and L. Gualtieri, *Gen. Relativ. Gravit.* **40**, 945 (2008).
- [53] E. Berti, V. Cardoso, and A. O. Starinets, *Classical Quantum Gravity* **26**, 163001 (2009).
- [54] E. Berti, V. Cardoso, and C. M. Will, *Phys. Rev. D* **73**, 064030 (2006).
- [55] J. Li, K. Lin, and N. Yang, *Eur. Phys. J. C* **75**, 131 (2015).
- [56] H. Ma and J. Li, *Chin. Phys. C* **44**, 095102 (2020).
- [57] D.-J. Liu, B. Yang, Y.-J. Zhai, and X.-Z. Li, *Classical Quantum Gravity* **29**, 145009 (2012).
- [58] S.-B. Chen and J.-L. Jing, *Classical Quantum Gravity* **22**, 533 (2005).
- [59] S.-B. Chen and J.-L. Jing, *Classical Quantum Gravity* **22**, 1129 (2005).
- [60] R. G. Daghigh and M. D. Green, *Classical Quantum Gravity* **26**, 125017 (2009).
- [61] R. G. Daghigh and M. D. Green, *Phys. Rev. D* **85**, 127501 (2012).
- [62] R. G. Daghigh, M. D. Green, J. C. Morey, and G. Kunstatter, *Phys. Rev. D* **102**, 104040 (2020).
- [63] A. Zhidenko, *Classical Quantum Gravity* **21**, 273 (2004).
- [64] A. Zhidenko, *Classical Quantum Gravity* **23**, 3155 (2006).
- [65] M. Chabab, H. El Moumni, S. Iraoui, and K. Masmar, *Astrophys. Space Sci.* **362**, 192 (2017).
- [66] S. Lepe and J. Saavedra, *Phys. Lett. B* **617**, 174 (2005).
- [67] P. A. González, E. Papantonopoulos, J. Saavedra, and Y. Vásquez, *Phys. Rev. D* **95**, 064046 (2017).
- [68] K. Lin and W.-L. Qian, *Classical Quantum Gravity* **34**, 095004 (2017).
- [69] R. A. Konoplya, *Phys. Rev. D* **68**, 024018 (2003).
- [70] D. Liu, Y. Yang, S. Wu, Y. Xing, Z. Xu, and Z.-W. Long, *Phys. Rev. D* **104**, 104042 (2021).
- [71] S. Chakraborty, K. Chakravarti, S. Bose, and S. SenGupta, *Phys. Rev. D* **97**, 104053 (2018).
- [72] A. K. Mishra, A. Ghosh, and S. Chakraborty, *Eur. Phys. J. C* **82**, 820 (2022).
- [73] S. W. Hawking, *Nature (London)* **248**, 30 (1974).
- [74] S. W. Hawking, *Commun. Math. Phys.* **43**, 199 (1975); **46**, 206(E) (1976).
- [75] S. Fernando, *Gen. Relativ. Gravit.* **37**, 461 (2005).
- [76] M. K. Parikh and F. Wilczek, *Phys. Rev. Lett.* **85**, 5042 (2000).
- [77] R. A. Konoplya, A. Zhidenko, and A. F. Zinhailo, *Classical Quantum Gravity* **36**, 155002 (2019).
- [78] P. Boonserm and M. Visser, *Phys. Rev. D* **78**, 101502 (2008).
- [79] P. Boonserm, T. Ngampitipan, and P. Wongjun, *Eur. Phys. J. C* **79**, 330 (2019).
- [80] M. Visser, *Phys. Rev. A* **59**, 427 (1999).
- [81] N. G. Sanchez, *Phys. Rev. D* **18**, 1030 (1978).
- [82] S. R. Das, G. W. Gibbons, and S. D. Mathur, *Phys. Rev. Lett.* **78**, 417 (1997).
- [83] Y. Decanini, A. Folacci, and B. Raffaelli, *Classical Quantum Gravity* **28**, 175021 (2011).
- [84] Y. Decanini, G. Esposito-Farese, and A. Folacci, *Phys. Rev. D* **83**, 044032 (2011).
- [85] R. T. Cavalcanti, R. C. de Paiva, and R. da Rocha, *Eur. Phys. J. Plus* **137**, 1185 (2022).
- [86] N. Dadhich, R. Maartens, P. Papadopoulos, and V. Rezania, *Phys. Lett. B* **487**, 1 (2000).
- [87] R. Moderski and M. Rogatko, *Phys. Rev. D* **64**, 044024 (2001).
- [88] R. Moderski and M. Rogatko, *Phys. Rev. D* **72**, 044027 (2005).
- [89] R. Moderski and M. Rogatko, *Phys. Rev. D* **63**, 084014 (2001).
- [90] S. Boudet, F. Bombacigno, G. J. Olmo, and P. J. Porfirio, *J. Cosmol. Astropart. Phys.* **05** (2022) 032.
- [91] E. Franzin, S. Liberati, J. Mazza, R. Dey, and S. Chakraborty, *Phys. Rev. D* **105**, 124051 (2022).
- [92] V. Cardoso and J. P. S. Lemos, *Phys. Rev. D* **64**, 084017 (2001).
- [93] T. Regge and J. A. Wheeler, *Phys. Rev.* **108**, 1063 (1957).
- [94] C. Gundlach, R. H. Price, and J. Pullin, *Phys. Rev. D* **49**, 883 (1994).
- [95] C. Gundlach, R. H. Price, and J. Pullin, *Phys. Rev. D* **49**, 890 (1994).
- [96] H.-J. Blome and B. Mashhoon, *Phys. Lett.* **100A**, 231 (1984).
- [97] G. Poschl and E. Teller, *Z. Phys.* **83**, 143 (1933).
- [98] R. A. Konoplya and A. Zhidenko, *Phys. Rev. D* **81**, 124036 (2010).
- [99] J. Matyjasek and M. Opala, *Phys. Rev. D* **96**, 024011 (2017).
- [100] S. Iyer and C. M. Will, *Phys. Rev. D* **35**, 3621 (1987).
- [101] B. F. Schutz and C. M. Will, *Astrophys. J. Lett.* **291**, L33 (1985).

- [102] K. D. Kokkotas and B. F. Schutz, *Phys. Rev. D* **37**, 3378 (1988).
- [103] E. Berti, V. Cardoso, J. A. Gonzalez, and U. Sperhake, *Phys. Rev. D* **75**, 124017 (2007).
- [104] S. Iyer, *Phys. Rev. D* **35**, 3632 (1987).
- [105] R. A. Konoplya, *Phys. Lett. B* **823**, 136734 (2021).
- [106] R. A. Konoplya and A. F. Zinhailo, *Phys. Rev. D* **99**, 104060 (2019).
- [107] S. Dey and S. Chakrabarti, *Eur. Phys. J. C* **79**, 504 (2019).
- [108] T. Ngampitipan and P. Boonserm, *Int. J. Mod. Phys. D* **22**, 1350058 (2013).
- [109] S. Barman, *Eur. Phys. J. C* **80**, 50 (2020).
- [110] M. Okyay and A. Övgün, *J. Cosmol. Astropart. Phys.* **01** (2022) 009.
- [111] W. Javed, I. Hussain, and A. Övgün, *Eur. Phys. J. Plus* **137**, 148 (2022).
- [112] W. Javed, M. Atique, and A. Övgün, *Gen. Relativ. Gravit.* **54**, 135 (2022).
- [113] R. C. Pantig and A. Övgün, *Ann. Phys. (Amsterdam)* **448**, 169197 (2023).
- [114] W. Javed, M. Aqib, and A. Övgün, *Phys. Lett. B* **829**, 137114 (2022).
- [115] F. Gray, S. Schuster, A. Van-Brunt, and M. Visser, *Classical Quantum Gravity* **33**, 115003 (2016).
- [116] R. B. Magalhães, L. C. S. Leite, and L. C. B. Crispino, *Eur. Phys. J. C* **80**, 386 (2020).
- [117] M. A. A. Paula, L. C. S. Leite, and L. C. B. Crispino, *Phys. Rev. D* **102**, 104033 (2020).
- [118] H. C. D. Lima, C. L. Benone, and L. C. B. Crispino, *Phys. Lett. B* **811**, 135921 (2020).
- [119] M. Dafermos, *Commun. Math. Phys.* **332**, 729 (2014).
- [120] H. Yang, A. Zimmerman, A. Zenginoğlu, F. Zhang, E. Berti, and Y. Chen, *Phys. Rev. D* **88**, 044047 (2013).
- [121] M. Richartz, *Phys. Rev. D* **93**, 064062 (2016).
- [122] A. Zimmerman and Z. Mark, *Phys. Rev. D* **93**, 044033 (2016); **93**, 089905(E) (2016).
- [123] S. Hod, *Eur. Phys. J. C* **77**, 351 (2017).
- [124] V. Cardoso, J. A. L. Costa, K. Destounis, P. Hintz, and A. Jansen, *Phys. Rev. Lett.* **120**, 031103 (2018).
- [125] V. Cardoso, J. L. Costa, K. Destounis, P. Hintz, and A. Jansen, *Phys. Rev. D* **98**, 104007 (2018).
- [126] O. J. C. Dias, H. S. Reall, and J. E. Santos, *J. High Energy Phys.* **10** (2018) 001.
- [127] K. Destounis, *Phys. Lett. B* **795**, 211 (2019).